



The evolution of pore structure heterogeneity during thermal maturation in lacustrine shale pyrolysis

Ming Guan^{a,b,c}, Xiaoping Liu^{a,b,*}, Zhijun Jin^{d,e,*}, Jin Lai^{b,c}, Biao Sun^{a,b}, Panpan Zhang^f, Kefei Chen^g

^a State Key Laboratory of Petroleum Resources and Prospecting, China University of Petroleum (Beijing), Beijing 102249, China

^b College of Geosciences, China University of Petroleum (Beijing), Beijing 102249, China

^c Research Institute of Petroleum Exploration and Development, China National Petroleum Corporation, Beijing 100083, China

^d Institute of Energy, Peking University, Beijing 100871, China

^e State Key Laboratory of Shale Oil and Gas Enrichment Mechanisms and Effective Development, Beijing 100083, China

^f School of Energy Resources, China University of Geosciences, Beijing 100083, China

^g National Institute of Natural Hazards, Ministry of Emergency Management of China, Beijing 100085, China

ARTICLE INFO

Keywords:

Shale
Pyrolysis
Thermal maturity
Pore structure heterogeneity
Evolution

ABSTRACT

Although pore structure variations during thermal maturation have been extensively discussed using natural or artificially matured shale samples, related investigations into pore structure heterogeneity and its evolution remain scarce, posing challenges in fine reservoir evaluation and exploration target prioritization. The variation of pore structure heterogeneity during thermal maturation was determined in this study by integrating multifractal theory with nitrogen adsorption-desorption tests using the naturally immature sample and the artificially matured samples, and the governing factors were ascertained. The increasing thermal maturity results in organic matter transformation, hydrocarbon generation, retention and expulsion, and various types of pore formation, driving the variation of pore structure heterogeneity. Pore structure heterogeneity, quantified by the breadth of singular spectra, was chiefly impacted by the pore volume difference between diverse types of pores. Macropores make a main contribution to pore structure heterogeneity due to their higher percentage of total pore volume compared to mesopores and micropores. Through a comparison of pore structure heterogeneity in shale samples with different thermal maturity, the impact of thermal maturity on shales was clarified. At immature to low-mature stages, nonthermal maturity factors make a main contribution to the inherent pore structure of different shales and cause an ambiguous relationship between pore structure heterogeneity and thermal maturity. At mature to high-mature stages, pore structure becomes more heterogeneous with increasing thermal maturity, resulting from newly formed organic pores or dissolution pores and the progressive generation and expulsion of liquid and gaseous hydrocarbons. At the over-mature stage, pore structure heterogeneity decreases and then fluctuates on a small scale, related to the collapse of mesopores and macropores caused by compaction and the predominance of newly formed micropores.

1. Introduction

Shales contain complicated pore systems with a wide spectrum of pore sizes, complex pore geometry, and diverse pore types, etc. [1,2], all of which are closely related to complicated pore structure and pore heterogeneity. The pore structure has a significant impact on the occurrence and fluidity of shale oil/gas in these pores [3–6], which is important when designing reservoir stimulation and predicting well

productivity [7,8].

A series of techniques have been employed to explore shale pore characteristics. 2D/3D imaging approaches are applied to characterize surface porosity, pore geometry, and pore connectivity [9,10], including light microscopy, scan electron microscopy, micro 3D X-ray microscopy, nano 3D X-ray microscopy, and focus ion beam-scan electron microscopy, etc. The pore structure of shale reservoirs can be evaluated using relevant parameters [11,12], such as surface area, pore volume, and

* Corresponding author at: College of Geosciences, China University of Petroleum (Beijing), Beijing 102249, China.

* Corresponding author at: Institute of Energy, Peking University, Beijing 100871, China.

E-mail addresses: liuxiaoping@cup.edu.cn (X. Liu), jinzj1957@pku.edu.cn (Z. Jin).

<https://doi.org/10.1016/j.jaap.2022.105501>

Received 19 November 2021; Received in revised form 13 February 2022; Accepted 10 March 2022

Available online 12 March 2022

0165-2370/© 2022 Elsevier B.V. All rights reserved.

pore size distribution, which can be acquired using gas adsorption (CO_2 , N_2 , Ar), mercury intrusion, nuclear magnetic resonance (NMR), and small/ultra-small angle neutron scattering, etc. Porosity and permeability can be determined by gas injection (He), fluid immersion, mercury intrusion, NMR, etc. [13,14]. Fractal features of shale pores have been explored by establishing a power-law relationship between scales (gas absorbed relative pressure, capillary pressure, transverse relaxation time) and the corresponding detecting volumes (gas adsorbed volume, mercury intrusion saturation, cumulative porosity), and the resulting fractal dimensions represent pore surface roughness and pore structural complexity. Multifractal theory, which specializes in capturing the local fluctuations and defining the heterogeneity of a system using a continuous dimension spectrum, has recently been successfully applied to quantify the variance of pore size distribution in shales. Pore structure heterogeneity of many shales globally has been quantified by processing pore images or pore structure data, including Bakken Fm in the Williston Basin [15,16], Kongdian Fm and Shahejie Fm in the Bahai Bay Basin [17, 18], Lucaogou Fm in the Junggar Basin [19], and Wufeng-longmaxi Fm in the Sichuan Basin [20–22], to evaluate reservoir types and qualities, explore governing mechanism of pore development, and compare the pore structure heterogeneity acquired from different methodologies or different shales.

The diagenesis and evolution of shales have been investigated by using natural samples or artificially matured samples, providing detailed insight into minerals transformation [7,23], kerogen structure changes [24–26], hydrocarbons generation-retention-expulsion [27–29], organic–inorganic interactions [30,31], and pore structure evolution [32–37]

during thermal maturation. Previous studies showed that thermal maturation has a positive impact on pore structure alternations in naturally or artificially matured samples [34,38], and concluded that shales with diverse organic matter types or mineral compositions demonstrate diversified pore structure evolution during thermal maturation [34,35]. During the process of hydrocarbon generation and expulsion, oil generative shales often exhibit a larger rise in pore volume and produce large-diameter pores, whereas gas generative shales readily form smaller-diameter pores [35,39]. Because of pore constructiveness or destruction induced by compaction, dissolution, and cementation in conventional reservoirs, pore variation in shale reservoirs is more intricate in view of the superimposition of diagenesis and thermal evolution [37,40]. However, research on the relationship between pore structure heterogeneity and hydrocarbon generation/expulsion during thermal maturation is scarce, which impedes the fine evaluation of shale reservoirs and the prediction of shale oil or shale gas occurrence.

In this study, various artificially matured shale samples were obtained from hydrous pyrolysis experiments, and pore structure heterogeneity was quantified by integrating multifractal analysis with nitrogen adsorption-desorption tests. Thermal maturation was established using the naturally immature lacustrine shale sample and its artificially matured counterparts to understand relationships among organic matter transformation, hydrocarbon generation-retention-expulsion, pore structure variation, and the corresponding heterogeneity. This study links variations in pore structure heterogeneity to the transformation of organic matter into petroleum and gas, and it has implications for prioritizing the key stage of oil and gas accumulation and favorable

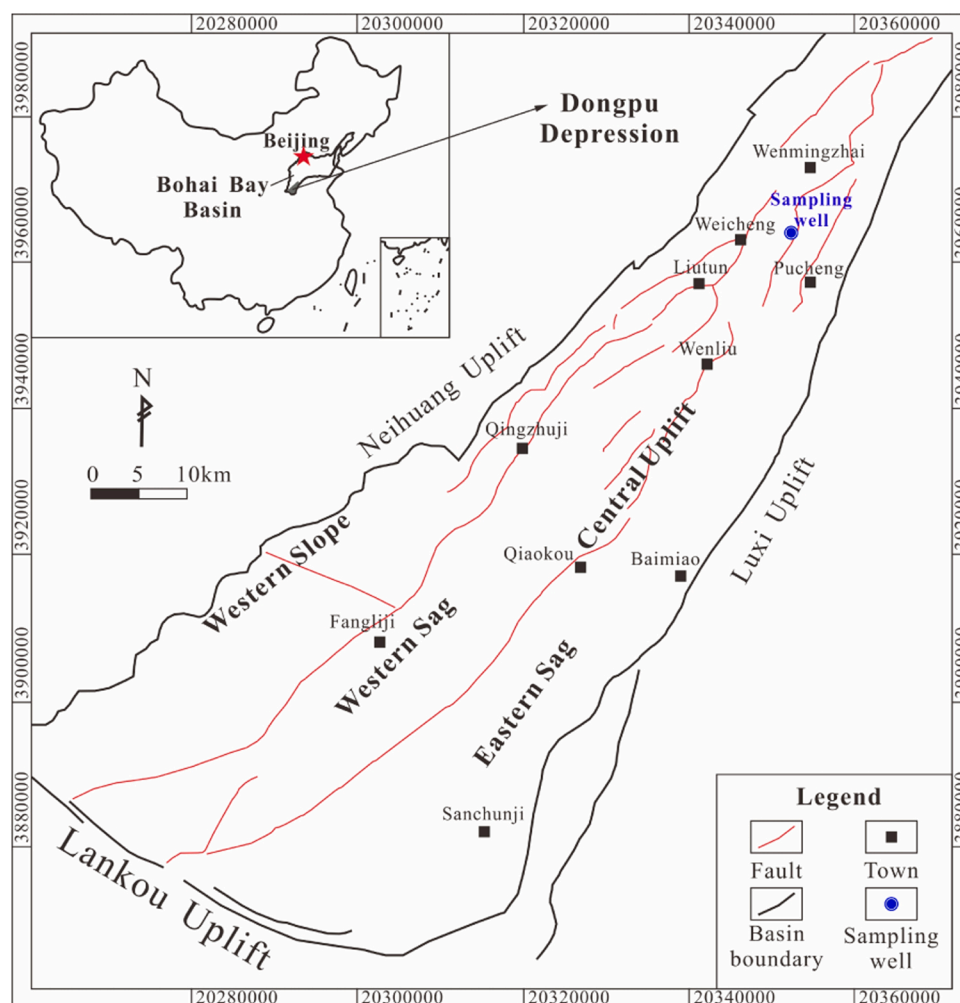


Fig. 1. The location and tectonic framework of the Dongpu Depression in Bohai Bay Basin, Eastern China [37], and sampling well location in this study.

reservoirs in self-sourced unconventional reservoirs.

2. Methodology

2.1. Samples

The organic-rich and immature shale sample with total organic carbon (TOC) of 1.77% and vitrinite reflectance (Ro) of 0.5% was collected from the Shahejie Fm in Dongpu Depression of the Bohai Bay Basin, Eastern China (Fig. 1). The shale is a potential source rock for the Dongpu Depression, with an average TOC value of 0.76%. As proven by the high percentage of exinite and sapropelinite, type II of organic matter predominates in the shale. The burial depth of the shale is mostly about 1800~2500 m, corresponding to immature to low-mature stages [41]. The sulfur-rich oil discovered in many regions of the Depression shows immature to low mature characteristics [42]. Six small core columns with a diameter of 3.8 cm and a height of 5 cm were drilled from the original sample to conduct hydrous pyrolysis.

2.2. Experiments

Semi-open pyrolysis experiments were conducted by a high-temperature/high-pressure autoclave from Sinopec Petroleum Exploration and Production Research Institute (Wuxi, China) [39]. The reactor was heated to 300, 325, 350, 375, 400, and 500 °C to obtain artificially matured shale samples with the various evolutionary stages of hydrocarbon generation, and the corresponding samples were named PY-300, PY-325, PY-350, PY-375, PY-400, and PY-500, respectively. The desired temperatures were achieved at a heating rate of 1 °C/min and then maintained for 48 h to ensure the thermal equilibrium of the entire system. Samples were saturated with high-pressure deionized water during the process of the pyrolysis experiments. Oil cylinders were used to provide the confining pressures. Pyrolysis products were collected and measured, including hydrocarbon products and sample residues.

The expelled gaseous mixture was identified and their relative contributions were determined by using a 3800 Gas Chromatograph, including H₂, O₂, N₂, CO₂, gaseous hydrocarbons (C_xH_{2x+2}, where 2 ≤ x ≤ 5), etc. The gaseous hydrocarbon amount was calculated according to the ideal gas law [43]. The amount of retained oil was determined in accordance with total solid residue weight and extractable organic matter (EOM) content that was extracted using the Soxhlet extraction procedure. Expelled liquid hydrocarbons were quantified by the liquid hydrocarbons collected from the oil collector and the autoclave wall and pipe. Total hydrocarbon amount was the sum of retained liquid hydrocarbons, expelled liquid hydrocarbons, and expelled gaseous hydrocarbons.

Shale samples were crushed into powder with a grain diameter of <80 mesh, and dilute hydrochloric acid was dropwise added into approximately 100 mg of powder samples to eliminate inorganic carbon. After that, the samples were introduced into a LECO CS-200 carbon/sulfur analyzer to measure TOC. Approximately 100 mg of powdered samples (< 100 mesh) were placed into a Rock-Eval 6 device to obtain pyrolysis parameters. Thin sections were produced by being coated with epoxy resin and polished, and Ro values were determined via an AxioSope.A1 microscope equipped with a photomicrometer and an oil immersion lens.

Powder samples (about 0.5 g, < 100 mesh) were degassed for 24 h at 423 K, and then a JWBK-200 C surface area/pore size analyzer was employed to obtain adsorption-desorption volumes of different relative pressures (P/P₀) with a range of 0.001~0.999 at -196 °C. Pores with a diameter of less than 200 nm were detected, and pores with different pore sizes were identified, including micropores (pore size < 2 nm), mesopores (pore size of 2~50 nm) and macropores (pore size > 50 nm) [44]. Subsequently, a series of pore structure parameters, including specific surface area, total pore volume, micropore volume, and pore size distribution (PSD), were calculated by the modified BET model

[45], the general principle of Gurevich rule [46], HK model [47], and BJH model [48], respectively.

2.3. Multifractal theory

The box-counting method was applied to nitrogen adsorption data to study the multifractal behavior of the shale. A set of different boxes with identical scale (r) were required to cover the total length of the target object. And then the total length was allocated to these boxes by a dyadic scaling down procedure. The density probability in ith box can be written as follows:

$$P_i(r) = V_i(r) / \sum_{i=1}^{N(r)} V_i(r) \quad (1)$$

where Pi(r) denotes the probability density function; Vi(r) represents the pore volume of ith box; N(r) is the total number of boxes, N(r) = 2^k (k = 0, 1, 2, ...). Pi(r), which fits an exponential function of r, can be expressed as [49]:

$$P_i(r) \propto r^{\alpha_i} \quad (2)$$

where α_i is the singularity exponent representing the singularity degrees of the system, and relates to number of the boxes N_α(r):

$$N_{\alpha}(r) \propto r^{-f(\alpha)} \quad (3)$$

where f(α) indicates the multifractal spectrum or singularity spectrum, meaning the same or close α values in these boxes. Thus, α(q) and f(α) can be calculated as below [50]:

$$\alpha(q) \propto \left[\sum_{i=1}^{N(r)} X_i(q, r) \times \log P_i(r) \right] / \log(r) \quad (4)$$

$$f(q) \propto \left[\sum_{i=1}^{N(r)} X_i(q, r) \times \log X_i(q, r) \right] / \log(r) \quad (5)$$

where X_i(q, r) is the partition function derived from the weighed sum of qth power of Pi(r) and also follows a power law function of r:

$$X_i(q, r) = \sum_{i=1}^{N(r)} P_i^q(r) \propto r^{\tau_q} \quad (6)$$

where q with a range of -10~10 in increments of 1 was used as exponents for scrutinizing the denser or sparser regions of measure μ_i(q, r) [51]; τ_q is the mass index and can be expressed as:

$$\tau_q = \lim_{r \rightarrow 0} \frac{\log \sum_{i=1}^{N(r)} P_i^q(r)}{\log(r)} \quad (7)$$

Generalized dimension D_q, referred to as singular measure [52], can be derived from:

$$D_q = \frac{1}{q-1} \lim_{r \rightarrow 0} \frac{\log \sum_{i=1}^{N(r)} P_i^q(r)}{\log(r)} = \frac{\tau(q)}{q-1} \quad (8)$$

In this study, multifractal properties were quantified by using the logarithmic form of P/P₀ and the density probability of gas adsorption volume derived from nitrogen adsorption-desorption results.

3. Results

3.1. Bulk organic geochemistry

The original sample is immature and has Ro of 0.50%. The desired experimental temperatures bring about an increase in thermal maturity ranging from 0.57% to 2.60% of Ro (Table 1), corresponding to thermal evolution from low-mature to over-mature stages. PY-300 with Ro of 0.57% is at the low mature stage; PY-325 and PY-350 with Ro values of 0.77% and 1.04%, respectively, are at the mature stage (i.e., the main

Table 1
Geochemical characteristics of original sample and artificially matured samples.

Sample ID.	Ro (%)	TOC (wt, %)	TS (wt, %)	S ₁ (mg/g)	S ₂ (mg/g)	T _{max} (°C)
Ori	0.50	1.77	1.54	0.33	8.64	430
PY-300	0.57	1.37	1.26	0.67	7.59	440
PY-325	0.77	1.34	1.21	1.47	5.81	443
PY-350	1.05	0.70	0.77	0.57	2.23	450
PY-375	1.42	0.60	0.64	0.16	0.23	430
PY-400	1.74	0.55	0.38	0.06	0.04	–
PY-500	2.60	0.74	1.03	0.02	0	–

“oil-window”); PY-375 and PY-400 with Ro of 1.42% and 1.74%, respectively, correspond to the high mature stage (i.e., the condensate and wet gas window); and PY-500 with Ro of 2.60% is at the overmature stage (i.e., the dry gas window).

TOC continues to decrease with increasing thermal maturity when Ro is less than 2.00%, resulting in about 70% of TOC depletion compared to the original sample. As thermal maturity increases, TOC rapidly decreases when Ro is less than 1.00%, slowly declines at Ro of 1.00%~2.00%, and eventually slightly increases when Ro is more than 2.00%. The small increase in TOC during the overmature stage could be attributed to the gaseous hydrocarbon expulsion and kerogen graphitization (Table 1, Fig. 2). Furthermore, a high total sulfur (TS) content was found in the original sample, and TS exhibits a similar tendency to TOC during thermal evolution, implying that sulfur is closely related to organic matter transformation. S₁ values first climb to their maximum at 350 °C, equivalent to Ro of 0.77%, and subsequently decrease as thermal maturity increases. S₂ values constantly decrease with advancing thermal maturity (Table 1, Fig. 2). The variations among TOC, S₁, and S₂ during thermal evolution result from the transformation of organic matters, hydrocarbon generation and expulsion, and the formation of pyrobitumen [53,54].

3.2. Hydrocarbon products

According to the variation of hydrocarbon products during the thermal evolution, three distinct hydrocarbon generation stages can be identified: the stage of increasing retained liquid hydrocarbons, the stage of increasing expelled liquid hydrocarbons, and the stage of increasing expelled gaseous hydrocarbons. During the stage of

increasing retained liquid hydrocarbons (0.50% < Ro ≤ 0.77%), the retained hydrocarbons dramatically increase and predominate in the total hydrocarbon generated, whereas expelled gas hydrocarbons and expelled liquid hydrocarbons exhibit a modest increase. During the stage of increasing expelled liquid hydrocarbons (0.77% < Ro ≤ 1.42%), expelled liquid hydrocarbons significantly increase, expelled gas hydrocarbons somewhat increase, whereas retained hydrocarbons decline sharply. Liquid hydrocarbons generated increase to their maximum at Ro of 1.04% and then decline as thermal maturity increases. Total hydrocarbons generated continuously increase when Ro is less than 1.04% and then stabilize after that. During the stage of increasing expelled gas hydrocarbons (1.42% < Ro), expelled gas dramatically increases, while liquid hydrocarbons generated and expelled decline, and retained liquid hydrocarbons maintain a low value near to 0 (Table 2, Fig. 3).

3.3. Pore structure characteristics

3.3.1. N₂ adsorption-desorption isotherms

Adsorption isotherms of all samples exhibit the II type feature with a pronounced knee-point at low P/P₀, which is related to the completion of monolayer coverage. The maximum adsorption volumes constantly increase as thermal maturity advances. Hysteresis loops formed by N₂ adsorption-desorption curves appear in all shale samples (Fig. 4). According to the updated classification from IUPAC [51], the original sample, PY-300, and PY-325 demonstrate a combination of the H3 and H4 types of the hysteresis loops (0.50% ≤ Ro ≤ 0.77%), PY-350 has a combination of the H2(b) and H3 types (Ro = 1.05%), and the other samples have the H2(b) type (1.42% ≤ Ro). H2(b) type of hysteresis

Table 2
Hydrocarbon products of the pyrolysis experiments.

Sample ID.	Total hydrocarbon yield (mgHC/gRock)	Liquid HC generated (mgHC/gRock)	Retained oil (mgHC/gRock)	Expelled oil (mgHC/gRock)	Expelled gas (mgHC/gRock)
PY-300	5.11	4.94	4.10	0.84	0.17
PY-325	7.48	7.11	5.93	1.18	0.37
PY-350	8.71	8.10	3.19	4.91	0.61
PY-375	8.68	7.80	0.62	7.18	0.88
PY-400	8.42	6.80	0.24	6.56	1.62
PY-500	8.81	3.81	0.05	3.76	4.99

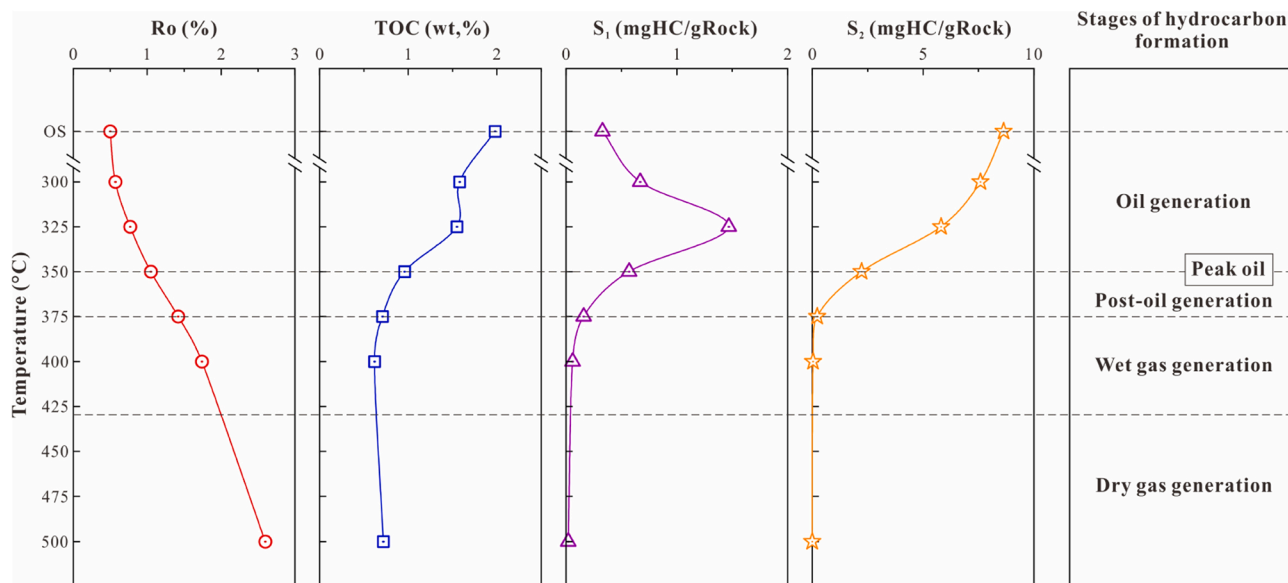


Fig. 2. Variations in geochemical indices of original shale sample and artificially matured samples showing that thermal maturation induces organic matter transformation and hydrocarbon generation.

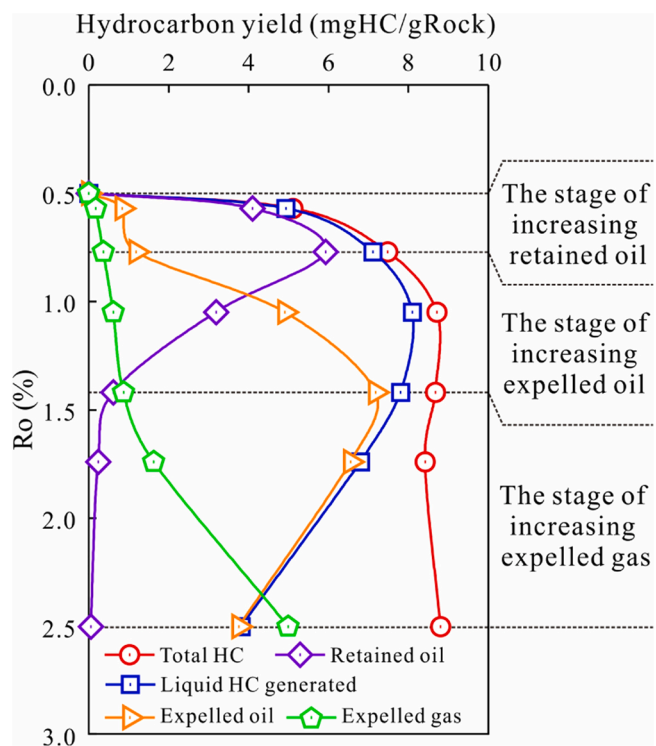


Fig. 3. Hydrocarbon products variation during the thermal evolution. Three different hydrocarbon generation stages can be identified by hydrocarbon products variation at different thermal maturity ranges, including the stage of increasing retained oil ($0.5\% < Ro \leq 0.77\%$), the stage of increasing expelled oil ($0.77\% < Ro \leq 1.42\%$), and the stage of expelled gas ($1.42\% < Ro$).

loops usually attribute to ink bottle pores with complex pore structure, such as narrow neck widths and large pore size; H3 type of hysteresis loops appear as a result of the silt-like shaped pores from some plate-like particles aggregates; and H4 type of hysteresis loops are usually associated with silt-like shaped pores with uniform size. Consequently, pores

in shales gradually change from silt-like shape to ink bottle shape with advancing thermal maturity.

During the process of thermal evolution, specific surface area and total pore volume overall increase with the increasing pyrolysis severity, which implies that newly formed pores change the pore structure of shale samples (Table 3). With increasing thermal maturity, the pore size distributions of all samples show a close resemblance in shape (Fig. 5). The pore volume increases overall as pyrolysis severity increases and reaches its maximum when pore diameter is near 200 nm. The increasing pyrolysis severity brings about an increase in pore volume (Table 3, Fig. 5). The volumes of micropores, mesopores, and macropores show different variations during thermal maturation. Micropore volume first declines at the low-mature stage and then continuously increases with increasing thermal maturity. At the low mature stage, newly formed pores are occluded by bitumen and thickened oil generated at this stage, resulting in a decrease in micropore volume [26,38]. Mesopore volume varies somewhat between $0.02 \text{ cm}^3/\text{g}$ and $0.03 \text{ cm}^3/\text{g}$ and reaches a maximum at $325 \text{ }^\circ\text{C}$ (0.77% of Ro). Macropore volume overall increases when thermal maturity is less than 2.00% and eventually decreases as thermal maturity further increases (Table 3, Fig. 6).

3.4. Multifractal characteristics

The monotonic, decreasing generalized dimensions spectra and convex parabola-like shaped singularity spectra derived from N_2 adsorption-desorption results justify the multifractal nature of these shale samples (Figs. 7 and 8). A series of parameters related to generalized dimension and singularity spectra are listed in Table 4. D_0 is termed capacity dimension or box dimension and represents fractal measure of the pore structure complexity [55]. D_1 and D_2 represent information dimension and correlation dimension, respectively [56]. The Hurst exponent (H), defined as $(D_2 + 1)/2$, can be used to describe pore connectivity [51]; the breadth of singularity spectra ($\Delta\alpha$) is quantified by the difference between α_{-10} and α_{10} , which can be utilized to quantify the pore structure heterogeneity [20,51]. The generalized dimension spectra are depicted in Fig. 7 and present a monotonic decreasing trend as q increases from -10 to 10 for all shale samples. PY-400 shows the largest amplitude difference of $D(q)$, implying the

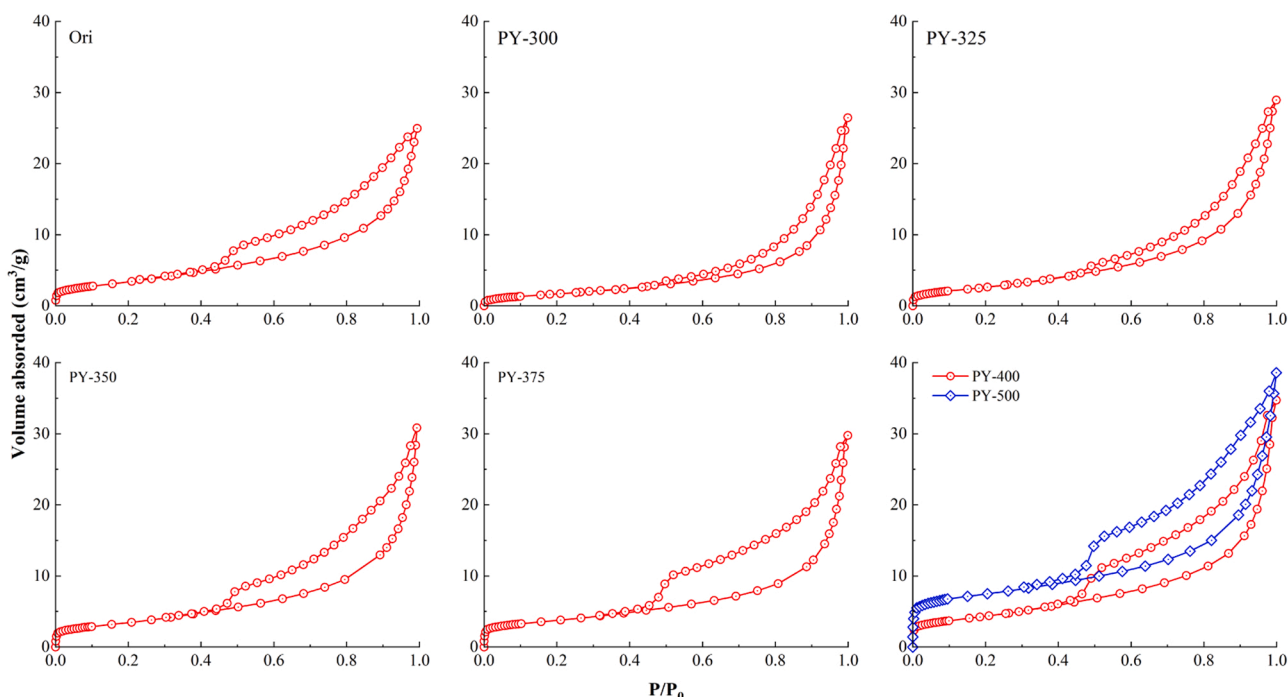


Fig. 4. Adsorption-desorption curves of original sample and artificially matured samples pyrolyzed at $300\text{--}500 \text{ }^\circ\text{C}$.

Table 3

Pore structure parameters of the original sample and artificially matured samples pyrolyzed at 300~500 °C.

Temperature (°C)	Ro (%)	Specific surface area (m ² /g)	Pore volume (cm ³ /g)			
			Total pore	Micropore	Mesopore	Macropore
-	0.50	12.418	0.039	0.005	0.024	0.010
300	0.57	6.724	0.041	0.002	0.022	0.017
325	0.77	10.441	0.045	0.004	0.029	0.012
350	1.05	12.383	0.048	0.005	0.025	0.017
375	1.42	13.209	0.046	0.005	0.021	0.020
400	1.74	15.404	0.054	0.006	0.028	0.034
500	2.60	27.263	0.060	0.011	0.026	0.023

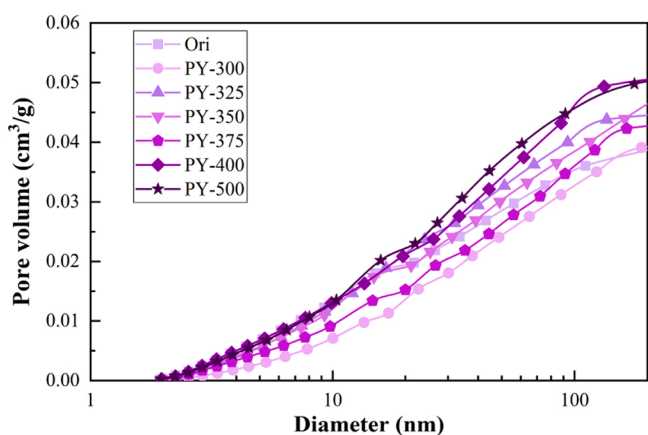


Fig. 5. Pore size distribution of original sample and artificially matured samples showing an increasing trend of pore volume with the increasing pyrolysis severity.

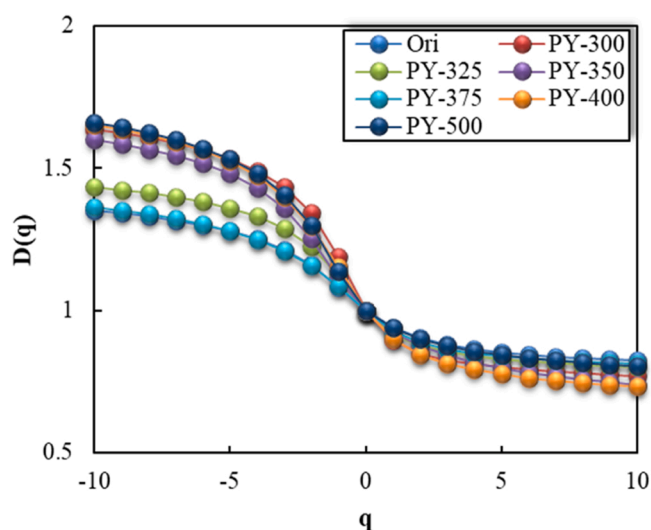


Fig. 7. Generalized dimension variation of the original sample and artificially matured samples pyrolyzed at 300~500 °C.

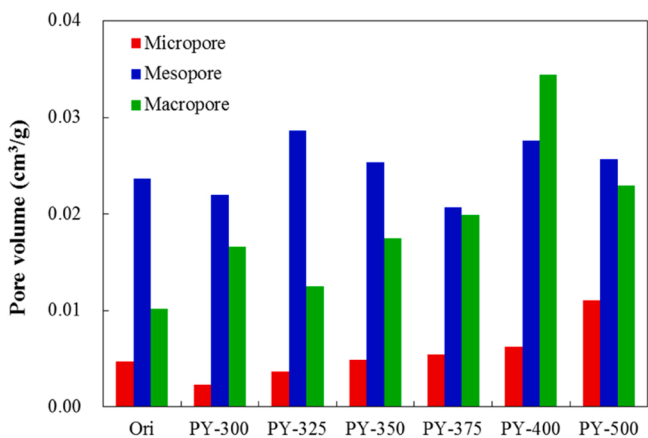


Fig. 6. Variation of different types of pore volumes from the original sample and artificially matured samples pyrolyzed at 300~500 °C.

most heterogeneous pore structure in PY-400. All samples have similar Hurst values that are near to 1, indicating good pore connectivity among different pores. Singularity spectra are displayed in Fig. 8, and all samples show a convex parabola-like shape. The $\Delta\alpha$ values vary from 0.664 to 1.130. The original sample, PY-325, and PY-375 have lower $\Delta\alpha$ values than other samples, indicating more homogeneous pore size distributions in those samples.

4. Discussion

4.1. The correlation among different factors during thermal maturation

The increasing thermal maturity results in organic matter

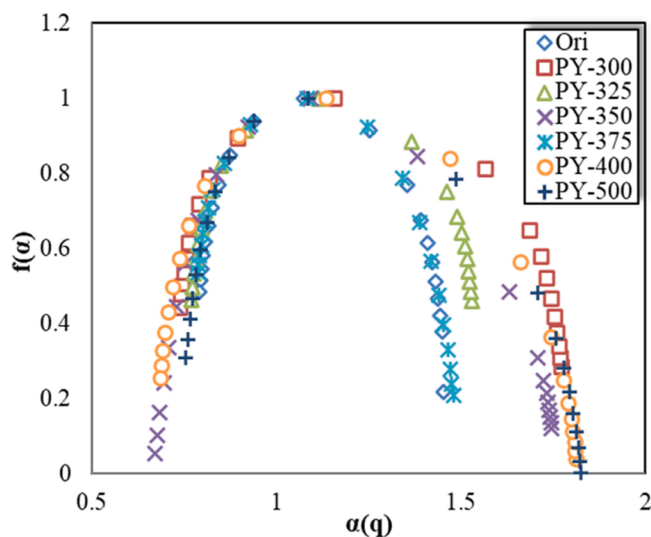


Fig. 8. Singularity spectra variation of the original sample and artificially matured samples pyrolyzed at 300~500 °C.

transformation, hydrocarbon generation-retention-expulsion, and diverse types of pore formation, driving the variation of pore structure heterogeneity. In this respect, Pearson correlation analysis was applied to help understand the relationships among different factors, including geochemical characteristics, thermal maturity, pore structure, and pore structure heterogeneity (Table 5). Obviously, the increasing pyrolysis severity contributes more to TOC, S_1 , micropore volume, macropore

Table 4

Multifractal parameters of the original sample and artificially matured shale samples pyrolyzed at 300~500 °C.

Sample ID.	Generalized dimension spectrum				Singularity Spectrum			
	D ₀	D ₁	D ₂	H	α ₁₀	α ₀	α ₁₀	Δα
Ori	1.000	0.939	0.903	0.951	1.454	1.076	0.790	0.664
PY-300	1.000	0.895	0.850	0.925	1.772	1.158	0.738	1.034
PY-325	1.000	0.916	0.876	0.938	1.531	1.114	0.768	0.763
PY-350	1.000	0.924	0.876	0.938	1.746	1.093	0.671	1.075
PY-375	1.000	0.929	0.888	0.944	1.479	1.084	0.787	0.693
PY-400	1.000	0.898	0.845	0.923	1.814	1.135	0.685	1.130
PY-500	1.000	0.939	0.902	0.951	1.826	1.088	0.754	1.072

volume, and specific surface area than pore structure heterogeneity and mesopore volume. The increasing thermal maturity causes decreasing TOC and variation of S₁, resulting from the hydrocarbon generation-retention-expulsion. The increasing thermal maturity also produces more pores, bringing about an increase in micropore, mesopore, and macropore volumes, especially for micropores and macropores. Micropore volume has a good positive correlation with Ro, implying an increasing number of micropores induced by thermal maturity. Furthermore, the close correlation between specific surface area and micropore volume demonstrates that micropores (< 2 nm) are the primary contributors to specific surface area in shale samples.

A good correlation between macropore volume and Δα suggests that macropores significantly impact the pore structure heterogeneity. When compared to micropores and mesopores, the increasing macropore volume usually has a high Δα value, resulting in more heterogeneous pore structure. Advanced thermal maturity increases pore structure heterogeneity, whereas TOC plays the opposite way. The variation of pore structure heterogeneity could be related to macropore volume changes caused by increasing pyrolysis severity and decreasing TOC.

4.2. The variation of pore structure heterogeneity

Pore structure heterogeneity quantified by Δα value was mostly impacted by the pore volume variations of different types of pores (Fig. 9). The larger the difference in pore volumes among various types of pores, the more heterogeneous the pore structure. The correlation between Δα and different pore volumes demonstrates that macropores play a significant role in pore structure heterogeneity.

During thermal evolution, pore structure heterogeneity varies dramatically due to the transformation of different types of pores and the retention or expulsion of oil and gas. The Δα value is lowest when Ro is 0.50%, indicating the less heterogeneous pore structure in the original sample with no or few hydrocarbons generated. At the low mature stage (0.50% < Ro < 0.77%), Δα value significantly increases at first, and then rapidly decreases. The transition from more to less heterogeneous pore structures in this stage results from the increase of the macropore volume and the decrease of the micropore and mesopore volumes.

Table 5

Correlation coefficients between pore structure heterogeneity parameters and governing factors.

	Δα	H	Ro (%)	TOC (wt %)	S ₁ (mg/g)	Micropore volume (cm ³ /g)	Mesopore volume (cm ³ /g)	Macropore volume (cm ³ /g)	Special surface area (m ² /g)
Δα	1.000	-0.535	0.469	-0.514	-0.272	0.281	0.273	0.662	0.303
H	-0.535	1.000	0.204	0.190	-0.174	0.536	-0.150	-0.478	0.505
Ro (%)	0.469	0.204	1.000	-0.731	-0.610	0.897	0.227	0.691	0.917
TOC (wt%)	-0.514	0.190	-0.731	1.000	0.485	-0.442	-0.063	-0.775	-0.455
S ₁ (mg/g)	-0.272	-0.174	-0.610	0.485	1.000	-0.562	0.347	-0.604	-0.575
Micropore volume (cm ³ /g)	0.281	0.536	0.897	-0.442	-0.562	1.000	0.287	0.395	0.997
Mesopore volume (cm ³ /g)	0.273	-0.150	0.227	-0.063	0.347	0.287	1.000	0.228	0.262
Macropore volume (cm ³ /g)	0.662	-0.478	0.691	-0.775	-0.604	0.395	0.228	1.000	0.423
Special surface area (m ² /g)	0.303	0.505	0.917	-0.455	-0.575	0.997	0.262	0.423	1.000

Micropore and mesopore might be occluded by the bitumen and density oil gradually generated at this stage [38,57,58]. An increase in macropore volume could be interpreted as pre-existing macropores in PY-300. At the main oil generation stage (0.77% ≤ Ro < 1.05%), Δα value rapidly increases due to a considerable difference in pore volumes among different types of pores and is related to increasing macropores and decreasing mesopores at this stage. Meanwhile, retained oil begins to decrease and expelled oil increases. Mesopore volume reaches its maximum when Ro is 0.77%, corresponding to the retained oil peak in the study, which could be attributed to organic acid-generated dissolution pores in minerals and organic pores formed from organic matter transformation. At the post-oil generation stage (1.05% ≤ Ro < 1.42%), the obvious decrease in mesopore volume might result from a decrease in retained oil and an increase in expelled oil, and macropores were gradually formed by those connected mesopores [59]. The low Δα value and the less heterogeneous pore structure are related to the similar pore volumes among different types of pores during this stage. The highest Δα value appears at the stage of wet gas generation (1.42% < Ro ≤ 2.00%), resulting from the large number of macropores generated by connecting micropores and mesopores after gas generation and expulsion [59]. At dry gas generation stage (2.00% < Ro), Δα value slightly declines, due to the similar pore volumes among different types of pores. At this stage, the porous solid bitumen from decomposition and condensation provides a large number of micropores [60], which has been found in many over-mature shales [61,62]; and the decrease in mesopore volume and macropore volume may be caused by compaction from confining pressure [60,63]. For shale oil exploration, the middle stage oil window, corresponding to Ro of 0.77%~1.20%, is more promising in terms of retained oil content, liquid hydrocarbon fluidity, and good pore structure. For gas counterparts, the stage of dry-gas generation is more favorable in terms of an increasing number of newly formed micropores, which provide the abundant surface area for the adsorption of methane.

4.3. Pore structure heterogeneity evolution based on a comparison

A comparison of Δα values of different shales covering thermal maturation was established to understand the impact of thermal

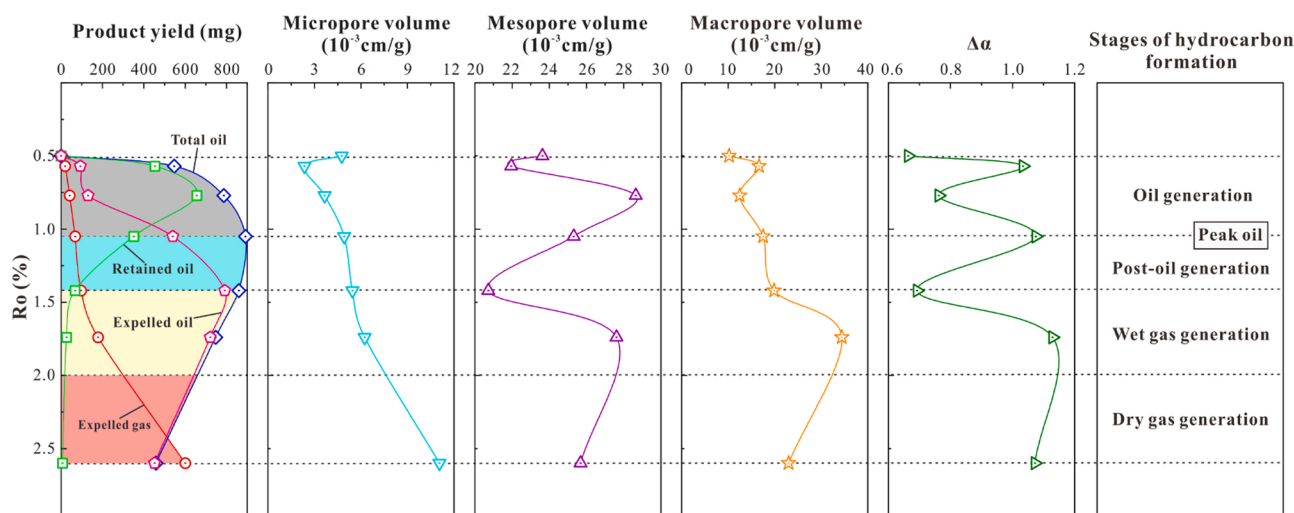


Fig. 9. Pore structure heterogeneity variation accompanied with hydrocarbon generation and expulsion and pore evolution during thermal maturation.

maturity on the pore structure heterogeneity of natural shale samples (Fig. 10). Nonthermal maturity factors, such as TOC, mineral components, and fabric, etc., contribute to the inherent pore structure in different shales with various rock compositions [62]. However, thermal maturity remains crucial in manipulating the whole process of diagenesis and hydrocarbon generation. As a result, the comparative result is still significant enough to provide a thorough understanding of how thermal maturation affects pore structural heterogeneity. At immature to low-mature stages, the relationship between pore structure heterogeneity and thermal maturity is ambiguous, and $\Delta\alpha$ values have a wide range from 0.24 to 1.034, with an average of 0.67. Compared with thermal maturity, other factors might make a main contribution to the inherent pore structure of different shales when R_o is less than 0.70%. At mature to high-mature stages, pore structure becomes more heterogeneous with increasing thermal stress, reaching the maximum heterogeneity at about 2.00% of R_o . The $\Delta\alpha$ values vary from 0.69 to 1.65 and have an average of 1.13. Increasing pore structure heterogeneity induced by increasing thermal stress is related to some new organic pores or dissolution pores and the progressive generation and expulsion of liquid and gaseous hydrocarbons throughout this stage. At the over-mature stage, $\Delta\alpha$ values vary from 0.31 to 1.07, with an average of 0.45. Pore heterogeneity decreases, and then fluctuates on a small scale. That might relate to the collapse of mesopores and macropores caused by compaction and the predominance of newly formed micropores in the

pore system at this stage.

During thermal evolution, pore structure heterogeneity varies dramatically due to the transformation of different types of pores and the retention or expulsion of oil and gas. The $\Delta\alpha$ value is lowest when R_o is 0.50%, indicating the less heterogeneous pore structure in the original sample with no or few hydrocarbons generated. At the low mature stage ($0.50\% < R_o < 0.77\%$), $\Delta\alpha$ value significantly increases at first, and then rapidly decreases. The transition from more to less heterogeneous pore structures in this stage results from the increase of the macropore volume and the decrease of the micropore and mesopore volumes. Micropore and mesopore might be occluded by the bitumen and density oil gradually generated at this stage [38,57,58]. An increase in macropore volume could be interpreted as pre-existing macropores in PY-300. At the main oil generation stage ($0.77\% \leq R_o < 1.05\%$), $\Delta\alpha$ value rapidly increases due to a considerable difference in pore volumes among different types of pores and is related to increasing macropores and decreasing mesopores at this stage. Meanwhile, retained oil begins to decrease and expelled oil increases. Mesopore volume reaches its maximum when R_o is 0.77%, corresponding to the retained oil peak in the study, which could be attributed to organic acid-generated dissolution pores in minerals and organic pores formed from organic matter transformation. At the post-oil generation stage ($1.05\% \leq R_o < 1.42\%$), the obvious decrease in mesopore volume might result from a decrease in retained oil and an increase in expelled oil, and macropores were gradually formed by those connected mesopores [59]. The low $\Delta\alpha$ value and the less heterogeneous pore structure are related to the similar pore volumes among different types of pores during this stage. The highest $\Delta\alpha$ value appears at the stage of wet gas generation ($1.42\% < R_o \leq 2.00\%$), resulting from the large number of macropores generated by connecting micropores and mesopores after gas generation and expulsion [59]. At the dry gas generation stage ($2.00\% < R_o$), $\Delta\alpha$ value slightly declines, due to the similar pore volumes among different types of pores. At this stage, the porous solid bitumen from decomposition and condensation provides a large number of micropores [60], which has been found in many over-mature shales [61,62]; and the decrease in mesopore volume and macropore volume may be caused by compaction from confining pressure [60]. For shale oil exploration, the middle stage oil window, corresponding to R_o of 0.77%~1.20%, is more promising in terms of retained oil content, liquid hydrocarbon fluidity, good pore structure. For gas counterparts, the stage of dry-gas generation is more favorable in terms of an increasing number of newly formed micropores, which provide the abundant surface area for the adsorption of methane.

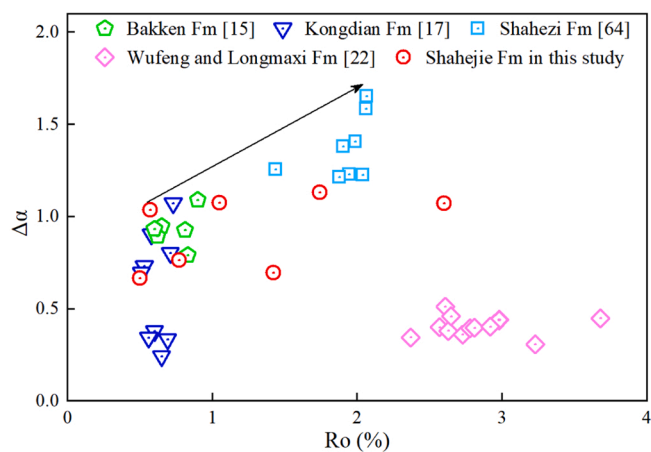


Fig. 10. Pore structure heterogeneity evolution of distinct shales with the increasing thermal maturity (The data of $\Delta\alpha$ and R_o in different shales from [15,17,22,64]).

4.4. Pore structure heterogeneity evolution based on a comparison

A comparison of $\Delta\alpha$ values of different shales covering thermal maturation was established to understand the impact of thermal maturity on the pore structure heterogeneity of natural shale samples (Fig. 10). Nonthermal maturity factors, such as TOC, mineral components, and fabric, etc., contribute to the inherent pore structure in different shales with various rock compositions [65]. However, thermal maturity remains crucial in manipulating the whole process of diagenesis and hydrocarbon generation. As a result, the comparative result is still significant enough to provide a thorough understanding of how thermal maturation affects pore structural heterogeneity. At immature to low-mature stages, the relationship between pore structure heterogeneity and thermal maturity is ambiguous, and $\Delta\alpha$ values have a wide range from 0.24 to 1.034, with an average of 0.67. Compared with thermal maturity, other factors might make a main contribution to the inherent pore structure of different shales when Ro is less than 0.70%. At mature to high-mature stages, pore structure becomes more heterogeneous with increasing thermal stress, reaching the maximum heterogeneity at about 2.00% of Ro. The $\Delta\alpha$ values vary from 0.69 to 1.65 and have an average of 1.13. Increasing pore structure heterogeneity induced by increasing thermal stress is related to some new organic pores or dissolution pores and the progressive generation and expulsion of liquid and gaseous hydrocarbons throughout this stage. At the over-mature stage, $\Delta\alpha$ values vary from 0.31 to 1.07, with an average of 0.45. Pore heterogeneity decreases, and then fluctuates on a small scale. That might relate to the collapse of mesopores and macropores caused by compaction and the predominance of newly formed micropores in the pore system at this stage.

5. Conclusion

The pore structure and its heterogeneity evolution were studied in the naturally immature shale sample and artificially matured shale samples by integrating the multifractal theory with N₂ adsorption results. Thermal maturation impacts organic matter transformation, hydrocarbon generation-retention-expulsion, and pore structure variation. In general, TOC decreases, S₁ attains the oil peak at 1.04% of Ro, and specific surface area and total pore volume increase as pyrolysis severity increases. However, the pore volumes of diverse types of pores are different. Micropore volume and macropore volume gradually increase with increasing thermal maturity, whereas the relationship between mesopore volume and Ro is ambiguous, resulting from the hydrocarbon generation-expulsion and newly formed mesopores.

Furthermore, pore structure heterogeneity is controlled by pore size distribution differentially constituted by micropores, mesopores, and macropores, causing a complicated change of pore structure heterogeneity during thermal maturation. Pore structure heterogeneity chiefly increases at mature to high-mature stages, closely related to newly formed organic pores or dissolution pores and the progressive generation and expulsion of liquid and gaseous hydrocarbons. This study provides new insight on pore structure evaluation during thermal maturation and has implications for the exploration prioritization of shale oil/gas in similar shales.

CRedit authorship contribution statement

Ming Guan: Conceptualization, Methodology, Formal analysis, Validation, Writing – original draft. **Xiaoping Liu:** Funding acquisition, Project administration, Writing – review & editing. **Zhijun Jin:** Project administration, Writing – review & editing. **Jin Lai:** Visualization, Investigation. **Biao Sun, Panpan Zhang, Kefei Chen:** Writing – review & editing.

Declaration of Competing Interest

The authors declare that they have no known competing financial interests or personal relationships that could have appeared to influence the work reported in this paper.

Acknowledgments

This work was supported by the National Natural Science Foundation of China [grant number 42072150, 41372144]; and the National Science and Technology Major Projects of China [grant number 2017ZX05049001-008]. We appreciate the enthusiastic support of Lunju Zheng at the Wuxi Institute of Petroleum Geology, SINOPEC Exploration and Development Research Institute. We acknowledge Prof. Haoquan Hu and two anonymous reviewers for their valuable comments and suggestions, which greatly improved the manuscript of an earlier version.

References

- [1] R.G. Loucks, R.M. Reed, S.C. Ruppel, U. Hammes, Spectrum of pore types and networks in mudrocks and a descriptive classification for matrix-related mudrock pores, *Aapg Bull.* 96 (2012) 1071–1098, <https://doi.org/10.1306/0817111061>.
- [2] A. Ougier-Simonin, F. Renard, C. Boehm, S. Vidal-Gilbert, Microfracturing and microporosity in shales, *Earth-Sci. Rev.* 162 (2016) 198–226, <https://doi.org/10.1016/j.earscirev.2016.09.006>.
- [3] T. Li, Z. Jiang, C. Xu, B. Liu, G. Liu, P. Wang, X. Li, W. Chen, C. Ning, Z. Wang, Effect of pore structure on shale oil accumulation in the lower third member of the Shahejie Formation, Zhanhua Sag, eastern China; Evidence from gas adsorption and nuclear magnetic resonance, *Mar. Pet. Geol.* 88 (2017) 932–949, <https://doi.org/10.1016/j.marpetgeo.2017.09.030>.
- [4] X. Liu, J. Lai, X. Fan, H. Shu, G. Wang, X. Ma, M. Liu, M. Guan, Y. Luo, Insights in the pore structure, fluid mobility and oiliness in oil shales of Paleogene Funing Formation in Subei Basin, China, *Mar. Pet. Geol.* 114 (2020), 104228, <https://doi.org/10.1016/j.marpetgeo.2020.104228>.
- [5] A.P. Radlinska, T. Blach, P. Vu, Y. Ji, L. de Campo, E.P. Gilbert, K. Regenauer-Lieb, M. Mastalerz, Pore accessibility and trapping of methane in Marcellus shale, *Int. J. Coal Geol.* (2021), 103850, <https://doi.org/10.1016/j.coal.2021.103850>.
- [6] C. Zhu, W. Guo, Y. Li, H. Gong, J.J. Sheng, M. Dong, Effect of occurrence states of fluid and pore structures on shale oil movability, *Fuel* 288 (2021), 119847, <https://doi.org/10.1016/j.fuel.2020.119847>.
- [7] D. Chandra, V. Vishal, A critical review on pore to continuum scale imaging techniques for enhanced shale gas recovery, *Earth-Sci. Rev.* 217 (2021), 103638, <https://doi.org/10.1016/j.earscirev.2021.103638>.
- [8] Y. Zhao, Z. Jin, Hydrocarbon mixture phase behavior in multi-scale systems in relation to shale oil recovery: The effect of pore size distributions, *Fuel* 291 (2021), 120141, <https://doi.org/10.1016/j.fuel.2021.120141>.
- [9] K.L. Milliken, M.E. Curtis, Imaging pores in sedimentary rocks: Foundation of porosity prediction, *Mar. Pet. Geol.* 73 (2016) 590–608, <https://doi.org/10.1016/j.marpetgeo.2016.03.020>.
- [10] R.E. Simon, S.C. Johnson, O. Khatib, M.B. Raschke, D.A. Budd, Correlative nano-spectroscopic imaging of heterogeneity in migrated petroleum in unconventional reservoir pores, *Fuel* 300 (2021), 120836, <https://doi.org/10.1016/j.fuel.2021.120836>.
- [11] C.R. Clarkson, N. Solano, R.M. Bustin, A.M.M. Bustin, G.R.L. Chalmers, L. He, Y. B. Melnichenko, A.P. Radlinski, T.P. Blach, Pore structure characterization of North American shale gas reservoirs using USANS/SANS, gas adsorption, and mercury intrusion, *Fuel* 103 (2013) 606–616, <https://doi.org/10.1016/j.fuel.2012.06.119>.
- [12] M. Wei, L. Zhang, Y. Xiong, J. Li, P. Peng, Nanopore structure characterization for organic-rich shale using the non-local-density functional theory by a combination of N₂ and CO₂ adsorption, *Micro Mesopor. Mat.* 227 (2016) 88–94, <https://doi.org/10.1016/j.micromeso.2016.02.050>.
- [13] L. Wang, D. Yang, Z. Kang, Evolution of permeability and mesostructure of oil shale exposed to high-temperature water vapor, *Fuel* 290 (2021), 119786, <https://doi.org/10.1016/j.fuel.2020.119786>.
- [14] A.T. Krzyzak, I. Habina-Skrzyniarz, G. Machowski, W. Mazur, Overcoming the barriers to the exploration of nanoporous shales porosity, *Micro Mesopor. Mat.* 298 (2020), 110003, <https://doi.org/10.1016/j.micromeso.2020.110003>.
- [15] K. Liu, M. Ostadhassan, L. Sun, J. Zou, Y. Yuan, T. Gentzis, Y. Zhang, H. Carvajal-Ortiz, R. Rezaee, A comprehensive pore structure study of the Bakken Shale with SANS, N₂ adsorption and mercury intrusion, *Fuel* 245 (2019) 274–285, <https://doi.org/10.1016/j.fuel.2019.01.174>.
- [16] P. Zhao, X. Wang, J. Cai, M. Luo, J. Zhang, Y. Liu, M. Rabiei, C. Li, Multifractal analysis of pore structure of Middle Bakken formation using low temperature N₂ adsorption and NMR measurements, *J. Pet. Sci. Eng.* 176 (2019) 312–320, <https://doi.org/10.1016/j.petrol.2019.01.040>.
- [17] M. Guan, X. Liu, Z. Jin, J. Lai, The heterogeneity of pore structure in lacustrine shales: Insights from multifractal analysis using N₂ adsorption and mercury intrusion, *Mar. Pet. Geol.* 114 (2020), 104150, <https://doi.org/10.1016/j.marpetgeo.2019.104150>.

- [18] M. Wang, C. Jiao, C. Li, N. Zhou, J. Li, S. Lu, F. Tian, G. Hao, J. Shi, Multi-fractal characteristics of micro-pores of Shahejie Formation shale in Dongying Sag, *Pet. Geol. Recovery Effic.* 26 (2020) 72–79.
- [19] P. Zhao, Z. Wang, Z. Sun, J. Cai, L. Wang, Investigation on the pore structure and multifractal characteristics of tight oil reservoirs using NMR measurements: Permian Lucaogou Formation in Jimusaer Sag, Junggar Basin, *Mar. Pet. Geol.* 86 (2017) 1067–1081, <https://doi.org/10.1016/j.marpetgeo.2017.07.011>.
- [20] K. Liu, M. Ostadhassan, L. Kong, Multifractal characteristics of Longmaxi Shale pore structures by N₂ adsorption: A model comparison, *J. Pet. Sci. Eng.* 168 (2018) 330–341, <https://doi.org/10.1016/j.petrol.2018.04.072>.
- [21] P. Wang, Z. Jiang, W. Ji, C. Zhang, Y. Yuan, L. Chen, L. Yin, Heterogeneity of intergranular, intraparticle and organic pores in Longmaxi Shale in Sichuan Basin, south China; Evidence from SEM digital images and fractal and multifractal geometries, *Mar. Pet. Geol.* 72 (2016) 122–138, <https://doi.org/10.1016/j.marpetgeo.2016.01.020>.
- [22] Y. Wang, H. Cheng, Q. Hu, L. Liu, L. Jia, S. Gao, Y. Wang, Pore structure heterogeneity of Wufeng-Longmaxi shale, Sichuan Basin, China: Evidence from gas physisorption and multifractal geometries, in: *J Petrol Sci Eng*, 208, 2022, <https://doi.org/10.1016/j.petrol.2021.109313>.
- [23] L. Xu, K. Yang, H. Wei, L. Liu, X. Li, L. Chen, T. Xu, X. Wang, Diagenetic evolution sequence and pore evolution model of Mesoproterozoic Xiamaling organic-rich shale in Zhangjiakou, Hebei, based on pyrolysis simulation experiments, *Mar. Pet. Geol.* 132 (2021), 105233, <https://doi.org/10.1016/j.marpetgeo.2021.105233>.
- [24] V. Agrawal, S. Sharma, Molecular characterization of kerogen and its implications for determining hydrocarbon potential, organic matter sources and thermal maturity in Marcellus Shale, *Fuel* 228 (2018) 429–437, <https://doi.org/10.1016/j.fuel.2018.04.053>.
- [25] S.R. Kelemen, M. Sansone, C.C. Walters, P.J. Kwiatek, T. Bolin, Thermal transformations of organic and inorganic sulfur in Type II kerogen quantified by S-XANES, *Geochim Cosmochim. Ac* 83 (2012) 61–78, <https://doi.org/10.1016/j.gca.2011.12.015>.
- [26] Y. You, X. Wang, X. Han, X. Jiang, Kerogen pyrolysis model based on its chemical structure for predicting product evolution, *Fuel* 246 (2019) 149–159, <https://doi.org/10.1016/j.fuel.2019.02.075>.
- [27] Z. Kang, Y. Zhao, D. Yang, L. Tian, X. Li, A pilot investigation of pyrolysis from oil and gas extraction from oil shale by in-situ superheated steam injection, *J. Pet. Sci. Eng.* 186 (2020), 106785, <https://doi.org/10.1016/j.petrol.2019.106785>.
- [28] L. Hou, W. Ma, X. Luo, J. Liu, S. Liu, Z. Zhao, Hydrocarbon generation-retention-expulsion mechanism and shale oil producibility of the permian lucaogou shale in the Junggar Basin as simulated by semi-open pyrolysis experiments, *Mar. Pet. Geol.* 125 (2021), 104880, <https://doi.org/10.1016/j.marpetgeo.2020.104880>.
- [29] X. Tang, J. Zhang, Z. Jiang, X. Zhao, K. Liu, R. Zhang, J. Xiong, K. Du, Z. Huang, J. Yu, Characteristics of solid residue, expelled and retained hydrocarbons of lacustrine marlstone based on semi-closed system hydrous pyrolysis: Implications for tight oil exploration, *Fuel (Guildf.)* 162 (2015) 186–193, <https://doi.org/10.1016/j.fuel.2015.09.009>.
- [30] G. Yuan, Y. Cao, N. Zan, S. Hans-Martin, G. Jon, F. Hao, Q. Jin, K. Liu, Y. Wang, Z. Chen, Z. Jia, Coupled mineral alteration and oil degradation in thermal oil-water-feldspar systems and implications for organic-inorganic interactions in hydrocarbon reservoirs, *Geochim Cosmochim. Ac* 248 (2019) 61–87, <https://doi.org/10.1016/j.gca.2019.01.001>.
- [31] X. Zhu, J. Cai, Y. Wang, H. Liu, S. Zhang, Evolution of organic-mineral interactions and implications for organic carbon occurrence and transformation in shale, *GSA Bull.* 132 (2019) 784–792, <https://doi.org/10.1130/B35223.1>.
- [32] L. Wang, Y. Zhao, D. Yang, Z. Kang, J. Zhao, Effect of pyrolysis on oil shale using superheated steam: A case study on the Fushun oil shale, China, *Fuel* 253 (2019) 1490–1498, <https://doi.org/10.1016/j.fuel.2019.05.134>.
- [33] Z. Kang, Y. Zhao, D. Yang, Review of oil shale in-situ conversion technology, *Appl. Energ.* 269 (2020), 115121, <https://doi.org/10.1016/j.apenergy.2020.115121>.
- [34] J. Chen, X. Xiao, Evolution of nanoporosity in organic-rich shales during thermal maturation, *Fuel* 129 (2014) 173–181, <https://doi.org/10.1016/j.fuel.2014.03.058>.
- [35] H. Guo, W. Jia, R. He, C. Yu, J. Song, P. Peng, Distinct evolution trends of nanometer-scale pores displayed by the pyrolysis of organic matter-rich lacustrine shales: Implications for the pore development mechanisms, *Mar. Pet. Geol.* 121 (2020), 104622, <https://doi.org/10.1016/j.marpetgeo.2020.104622>.
- [36] L.T. Ko, S.C. Ruppel, R.G. Loucks, P.C. Hackley, T. Zhang, S. Deyong, T. Gentzsis, J. O'Keefe, J. Curiale, T. Demchuk, Pore-types and pore-network evolution in Upper Devonian-Lower Mississippian Woodford and Mississippian Barnett mudstones; Insights from laboratory thermal maturation and organic petrology, *Int J. Coal Geol.* 190 (2018) 3–28, <https://doi.org/10.1016/j.coal.2017.10.001>.
- [37] M. Mastalerz, A. Schimmelmann, A. Drobniak, Y. Chen, Porosity of Devonian and Mississippian New Albany Shale across a maturation gradient: Insights from organic petrology, gas adsorption, and mercury intrusion, *Aapg Bull.* 97 (2013) 1621–1643, <https://doi.org/10.1306/04011312194>.
- [38] S. Zargari, K.L. Canter, M. Prasad, Porosity evolution in oil-prone source rocks, *Fuel* 153 (2015) 110–117, <https://doi.org/10.1016/j.fuel.2015.02.072>.
- [39] S. Wu, Z. Yang, X. Zhai, J. Cui, L. Bai, S. Pan, J. Cui, An experimental study of organic matter, minerals and porosity evolution in shales within high-temperature and high-pressure constraints, *Mar. Pet. Geol.* 102 (2019) 377–390, <https://doi.org/10.1016/j.marpetgeo.2018.12.014>.
- [40] T. Cao, M. Deng, Q. Cao, Y. Huang, Y. Yu, X. Cao, Pore formation and evolution of organic-rich shale during the entire hydrocarbon generation process: Examination of artificially and naturally matured samples, *J. Nat. Gas. Sci. Eng.* 93 (2021), 104020, <https://doi.org/10.1016/j.jngse.2021.104020>.
- [41] Q. Zhang, Z. Shen, Y. Chen, W. Wang, The evaluation of hydrocarbon-generating ability in Member 1 of Shahejie Formation of Dongpu Sag, China, *J. Chengdu Univ. Technol. (Sci. Technol. Ed.)* 34 (2007) 69–72.
- [42] C. Ke, S. Li, H. Zhang, N. He, K. Grice, T. Xu, P. Greenwood, Compound specific sulfur isotopes of saline lacustrine oils from the Dongpu Depression, Bohai Bay Basin, NE China, *J. Asian Earth Sci.* 195 (2020), 104361, <https://doi.org/10.1016/j.jseas.2020.104361>.
- [43] A.L.D. Spigolon, M.D. Lewan, H.L. de Barros Penteado, L.F.C. Coutinho, J. G. Mendonca Filho, Evaluation of the petroleum composition and quality with increasing thermal maturity as simulated by hydrous pyrolysis; A case study using a Brazilian source rock with Type I kerogen, *Org. Geochem* 83–84 (2015) 27–53, <https://doi.org/10.1016/j.orggeochem.2015.03.001>.
- [44] K.S.W. Sing, Reporting physisorption data for Gas/Solid systems with special reference to the determination of surface area and porosity, *Pure Appl. Chem.* 54 (1982) 2201–2218, <https://doi.org/10.1351/pac198254112201>.
- [45] J. Rouquerol, P. Llewellyn, F. Rouquerol, Is the BET equation applicable to microporous adsorbents? *Stud. Surf. Sci. Catal.* 160 (2007) 49–56.
- [46] F. Rouquerol, J. Rouquerol, K. Sing, *Adsorption by Powders and Porous Solids, second ed.*, Academic Press., New York, 1999.
- [47] G. Horvath, K. Kawazoe, Method for the calculation of effective pore size distribution in molecular sieve carbon, *J. Chem. Eng. Jpn* 16 (1983) 470–475.
- [48] E.P. Barrett, L.G. Joyner, P.P. Halenda, The determination of pore volume and area distribution in porous substances. I. Computations from nitrogen isotherms, *J. Am. Chem. Soc.* 73 (1951) 373–380, <https://doi.org/10.1021/ja01145a126>.
- [49] T.C. Halsey, M.H. Jensen, L.P. Kadanoff, I. Procaccia, B.I. Shraimant, Fractal measures and their singularities: The characterization of strange sets, *Phys. Rev. a* 33 (1986) 1141–1151.
- [50] A. Chhabra, R.V. Jensen, Direct determination of the $f(\alpha)$ singularity spectrum, *Phys. Rev. Lett.* 62 (1989) 1327–1330.
- [51] F. San José Martínez, M.A. Martín, F.J. Caniego, M. Tuller, A. Guber, Y. Pachepsky, C. García-Gutiérrez, Multifractal analysis of discretized X-ray CT images for the characterization of soil macropore structures, *Geoderma* 156 (2010) 32–42, <https://doi.org/10.1016/j.geoderma.2010.01.004>.
- [52] P. Grassberger, Generalized dimensions of strange attractors, *Phys. Lett. a* 97 (1983).
- [53] M. Mastalerz, A. Drobniak, A.B. Stankiewicz, Origin, properties, and implications of solid bitumen in source-rock reservoirs: A review, *Int J. Coal Geol.* 195 (2018) 14–36, <https://doi.org/10.1016/j.coal.2018.05.013>.
- [54] B.P. Tissot, R. Pelet, P. Ungerer, Thermal history of sedimentary basins, maturation indices, and kinetics of oil and gas generation, *Aapg Bull.* 71 (1987) 1445–1466, <https://doi.org/10.1306/703C80E7-1707-11D7-8645000102C1865D>.
- [55] F.J. Caniego, M.A. Martí, F. San Jose, M. van Meirvenne, P. Govaerts, Rényi dimensions of soil pore size distribution, *Geoderma* 112 (2003) 205–216, [https://doi.org/10.1016/S0016-7061\(02\)00307-5](https://doi.org/10.1016/S0016-7061(02)00307-5).
- [56] J.P. Ferreira, M. Wilson, E.V. Vázquez, Multifractal description of nitrogen adsorption isotherms, *Vadose Zone J.* 8 (2009) 209–219.
- [57] Y. Han, B. Horsfield, R. Wirth, N. Mahlstedt, S. Bernard, Oil retention and porosity evolution in organic-rich shales, *Aapg Bull.* 101 (2017) 807–827, <https://doi.org/10.1306/09221616069>.
- [58] S.C. Löhr, E.T. Baruch, P.A. Hall, M.J. Kennedy, Is organic pore development in gas shales influenced by the primary porosity and structure of thermally immature organic matter? *Org. Geochem* 87 (2015) 119–132, <https://doi.org/10.1016/j.orggeochem.2015.07.010>.
- [59] C. Huang, Y. Ju, H. Zhu, G.G. Lash, Y. Qi, K. Yu, H. Feng, L. Ju, P. Qiao, Investigation of formation and evolution of organic matter pores in marine shale by helium ion microscope: An example from the Lower Silurian Longmaxi Shale, South China, *Mar. Pet. Geol.* 120 (2020), 104550, <https://doi.org/10.1016/j.marpetgeo.2020.104550>.
- [60] T. Borjigin, L. Lu, L. Yu, W. Zhang, A. Pan, B. Shen, Y. Wang, Y. Yang, Z. Gao, Formation, preservation and connectivity control of organic pores in shale, *Pet. Explor. Dev.* 48 (2021) 798–812, [https://doi.org/10.1016/S1876-3804\(21\)60067-8](https://doi.org/10.1016/S1876-3804(21)60067-8).
- [61] M.E. Curtis, B.J. Cardott, C.H. Sondergeld, C.S. Rai, Development of organic porosity in the Woodford Shale with increasing thermal maturity, *Int J. Coal Geol.* 103 (2012) 26–31, <https://doi.org/10.1016/j.coal.2012.08.004>.
- [62] Y. Wang, L. Wang, J. Wang, Z. Jiang, C. Jin, Y. Wang, Characterization of organic matter pores in typical marine and terrestrial shales, China, *J. Nat. Gas. Sci. Eng.* 49 (2018) 56–65, <https://doi.org/10.1016/j.jngse.2017.11.002>.
- [63] G. Hu, Q. Pang, K. Jiao, C. Hu, Z. Liao, Development of organic pores in the Longmaxi Formation overmature shales: Combined effects of thermal maturity and organic matter composition, *Mar. Pet. Geol.* 116 (2020), 104314, <https://doi.org/10.1016/j.marpetgeo.2020.104314>.
- [64] Z. Liang, Z. Li, L. Li, Z. Jiang, D. Liu, F. Gao, X. Liu, L. Xiao, Y. Yang, Relationship between multifractal characteristics of pore size and lithofacies of shale of Shahezi Formation in Changling fault depression, Songliao Basin, *Lithol. Reserv.* 32 (2020) 22–35.
- [65] D. Gafurova, A. Kalmykov, D. Korost, G. Kalmykov, Macropores generation in the domanic formation shales: Insights from pyrolysis experiments, *Fuel* 289 (2021), 119933, <https://doi.org/10.1016/j.fuel.2020.119933>.